Active Solar Chimney (ASC) - Numerical and experimental study of energy storage and evaporative cooling

José Carlos Frutos Dordelly[1], Mike Coillot[1], Mohamed El Mankibi[1], Ricardo Enriquez Miranda[2], Maria José Jimenez[2], Jesus Arce Landa[3]

[1] ENTPE – Université de Lyon, Vaulx-en-Velin (France)

[2] CIEMAT, Almeria (Spain)

[3] CENIDET – Cuernavaca (Mexico)

Abstract

Research in the domain of renewable energies has been showing increasing consideration of energetic sustainability due to the escalation of global environmental concern. This paper focuses on implementing an energy storage solution in a hybrid ventilation system. Solar Chimneys constitute an effective technology used in green building architecture that capitalizes on solar energy to provide thermal comfort and air quality. The study centers on the effects of the organic paraffinic Phase Changing Material (PCM) RT-44 panel upon the thermal performance of a laboratory prototype and a stand-alone solar chimney. Furthermore, a numerical model has been established, which solves the thermal exchange of a PCM integrated multi-layered wall. The mass balance of the aerodynamic model of the chimney channel is calculated and input into a coupled model.

Keywords: energy storage, green energy, green house emission, PCM, solar chimney

1. Introduction

For the past years, natural ventilation has increasingly taken into consideration new energy-efficient strategies for thermal comfort as well as air quality improvement. One of the main objectives of the COP21 – Sustainable Innovation Forum meetings (information available at: http://www.cop21paris.org/) has been to decrease energetic consumption and to implement of green energies in order to reduce greenhouse gas emissions.

1.1 Overview

In its simplest design, a Solar Chimney is a channel used to evacuate hot air from a building via a closed conduct at a higher elevation. By means of the greenhouse effect, temperature rises across the canal and induces a thermal updraft. Most recent designs, as the one proposed by Arce, Jiménez, *et al.*, 2009, have made modifications to add elements such as a glazing or an opposite collector wall, both of which maximize the incoming solar energy and improve the chimney's performance. The use of solar chimneys is only profitable during the day, when solar energy heats the chimney and the air within it. Thus far, the induced airflow created in the chimney has been used for ventilation almost exclusively in hot countries.

The chimney acts like a heat engine converting heat generated by a collector into kinetic flow. The main task of the collector is to absorb solar energy for heating air and release it as solar radiation decreases. The initial driver of a solar chimney is the temperature difference between the inside of the building and the inside of the conduit, which causes a density variation. Several previous studies (Bansal, Mathur and Bhandari, 1993; Mathur *et al.*, 2006; Jianliu and Weihua, 2013; Naraghi and Blanchard, 2015) have proven that mass flow rate is directly related to solar radiation. Other investigations focused on the effect of solar radiation intensifiers on the performance of solar chimneys (Shahreza and Imani, 2015), however few have investigated the possibility of after-sundown utilization or the possibility of implementing this ventilation system in cold climate environments.

1.2 Active Solar Chimney

The objective of the study is to analyze the effectiveness of energy storage devices, in particular organic phase changing materials (PCMs), on solar chimneys for after-sundown utilization. The activation (transition from passive to PCM enhanced ventilation) of this technology is achieved through the implementation of these PCM panels.

The interest of phase changing materials lies in their superior energy storage capacity per unit of volume in

doi:10.18086/swc.2017.12.03 Available at http://proceedings.ises.org

comparison to conventional building materials. This type of material stores energy in its latent form. A rise in temperature up to the range of 40 – 44 °C will induce a change of state of the material from solid to liquid. The melting phase is an endothermic process, where heat is absorbed for the phase changing. Furthermore, the stored energy is released during the solidification process once temperature drops. The selected RT44 PCM panel has a heat storage capacity of 250 kJ/kg (or 70 Wh/kg) for a combination of latent and sensible heat in a temperature range of 35°C to 50°C.

Overall, paraffinic phase change materials for implementation in solar chimneys could be an economically viable option for hybrid design solutions to create a healthy indoor environment within residential buildings through renewable solar energy. The aim if this analysis is to evaluate the thermal performance of PCMs for residential purposes particularly after sundown.

Fig.1a represents a simple solar chimney as developed by Arce *et al.*, 2015, which is the basis of our model that integrates the PCM panels as shown in Fig.1b. This study will focus on the macro encapsulated organic PCM panels (bottom) filled with RT44 (top) shown in Fig.1c.

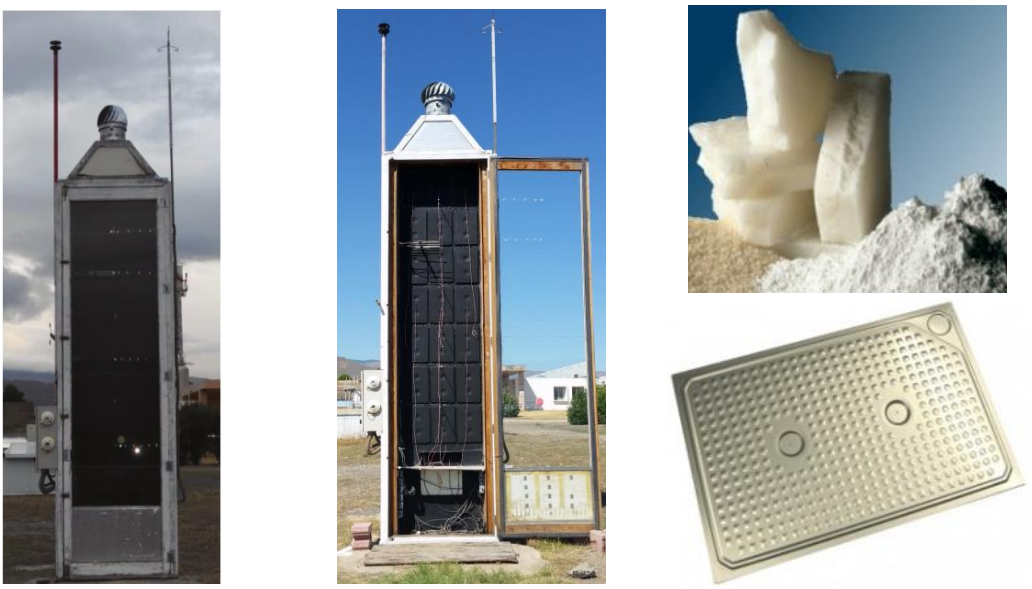

(a) **(b)** **(c)**

Figure 1: (a) Solar chimney built by Arce et al. (b) PCM panel integrated solar chimney. (c) Top - Organic paraffinic PCM in solid state. Bottom - macroencapsulated panel.

2. Numerical approach

The system is modeled by a heat transfer model and a pressure code. The first model integrates a multi-layered wall containing PCM and the second by analyzes the air temperature, speed and pressure distribution.

2.1 PCM integrated multi-layered wall

The model was developed using a finite-difference Crank-Nicholson implicit method, which follows a central difference scheme at time $t_{n+1/2}$ and a second order central difference for the space derivative at position x_i by setting the new variable $\bar{T}$:

$$\bar{T}_i = \frac{T_i^{t+\Delta t} + T_i^t}{2} \qquad (eq.1)$$

This method was chosen over other finite-differences approaches due to its faster convergence and its superior stability properties, especially at higher time steps (Δt) however, at the expense of a higher computational cost. Since we test our system over a large time interval, stability must be assured. Unstable approaches are not well suited due to these large time steps. The following expressions allows us to define a mathematical resolution that considers four different types of nodes: nodes in contact with the exterior environment, nodes in contact

with the internal channel, nodes within a solid material and the nodes in the interfaces between materials. The system is defined as follows:

$$\begin{cases} T_1^t = \left(1 + \frac{\lambda_1\gamma_1\Delta t_1}{\Delta x_1^2} + \frac{h_{ext}\gamma_1\Delta t_1}{\Delta x_1}\right)\bar{T}_1 + \frac{\lambda_1\gamma_1\Delta t_1}{\Delta x_1^2}\bar{T}_2 - \frac{h_{ext}\gamma_1\Delta t_1}{\Delta x_1}T_{ext} - \frac{\gamma_1\Delta t_1}{\Delta x_1}\left(\alpha_{clo}\varphi_{clo} + \alpha_{glo}\varphi_{glo}\right) & (eq.2) \\ T_i^t = -\frac{\lambda_i\gamma_i\Delta t_i}{2\Delta x_i^2}\bar{T}_{i-1} + \left(1 + \frac{\lambda_i\gamma_i\Delta t_i}{\Delta x_i^2}\right)\bar{T}_i - \frac{\lambda_i\gamma_i\Delta t_i}{2\Delta x_i^2}\bar{T}_{i+1} & (eq.3) \\ T_j^t = -\frac{\lambda_{j-1}\Delta t_{j-1}}{\vartheta\Delta x_{j-1}^2}\bar{T}_{j-1} + \left(1 + \frac{\lambda_{j-1}\Delta t_{j-1}}{\vartheta\Delta x_{j-1}^2} + \frac{\lambda_{j+1}\Delta t_{j+1}}{\vartheta\Delta x_{j+1}^2}\right)\bar{T}_j - \frac{\lambda_{j+1}\Delta t_{j+1}}{\vartheta\Delta x_{j+1}^2}\bar{T}_{j+1} & (eq.4) \\ T_n^t = -\frac{\lambda_n\gamma_n\Delta t_n}{\Delta x_n^2}\bar{T}_{n-1} + \left(1 + \frac{\lambda_n\gamma_n\Delta t_n}{\Delta x_n^2} + \frac{h_{int}\gamma_n\Delta t_n}{\Delta x_n}\right)\bar{T}_n - \frac{h_{int}\gamma_n\Delta t_n}{\Delta x_n}T_{int} - \frac{\gamma_n\Delta t_n}{\Delta x_n}\left(\alpha_{clo}\varphi_{clo} + \alpha_{glo}\varphi_{glo}\right) & (eq.5) \end{cases}$$

Eqs. 2-5 are solved by the following matricial equation and solving for $T_i^{t+\Delta t}$ in the previous eq.1:

$$T_i^t = A\bar{T} + Bu \qquad (eq.6)$$

2.2 Modelling of PCM Non-linearity in a multi-layered wall

In order to account for the non-linear behavior of phase changing materials, several options were considered. Some studies have explained the behavior of phase changing materials by setting three different working phases: solid, liquid and transitory state (Li and Liu, 2014). Studies such as the one carried out by Mirzaei and Haghighat, 2012 have modelled the behavior in similar ways and adding a discretization along the PCM layer to simulate the progressive phase change of the material. Other articles have opted to work on different approaches such as DTA (Differential thermal analysis) (Zhou, Zhao and Tian, 2012) and DSC (Differential scanning calorimetry) tests (Kheradmand *et al.*, 2016), both techniques in which the difference in the amount of heat required to increase the temperature of a sample and reference is measured as a function of temperature. This last technique was chosen over other options since the data from the test can be simply input into the code instead of calculated at each time interval; thus reducing the calculation time of the numerical model.

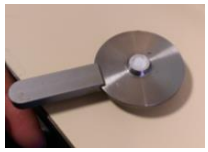

(a)

(b)

(c)

Figure 2: (a) Preparation of solid state RT44 material. (b) Sample setup for DSC analysis. (c) DSC test machine

The results of the DSC test for the Rubitherm RT44 phase changing material are shown in Fig.3. This test was carried out at a cooling/heating speed of 0.05°C/min, according to the expected charge/discharge speed of the panels in the chimney. The specific heat of the RT44 material is input to each node of the discretization as a function of temperature $C_p(T)$, allowing a more specific evolution along the PCM layer. Specific heat is calculated using the following expression:

$$C_p(T) = \frac{DSC(T)_s}{\varphi} \qquad (eq.7)$$

2.3 Pressure code – Airflow calculation model

The aerodynamic behavior and the heat exchange of the fluid within the conduct are influenced by the boundary wall temperature. This model employs a pressure code for the calculation of airflows throughout the

conduct and is based on the following simplifications:

- Airflow through the channel has been assumed one-dimensional. Only the vertical component parallel to the height of the chimney are considered.
- No losses are considered throughout the air channel. The mass conservation equations only take into account the exchanges between adjacent volumes and boundaries.
- Density is not constant and behaves according to the Boussinesq approximation as a function of temperature to account for the buoyancy driven flow.

The pressure code follows an iterative resolution based on the Newton-Raphson method. The mass balance $\dot{m}$ of a cell i connected to cells j of a domain is expressed by the following equation:

$$\sum_{k=1}^{j} \dot{m}_{ik} = 0 \qquad (eq.8)$$

The mass flow rate depends on the pressures of the neighboring cells. The mass exchange between common interfaces will serve to calculate the new pressure distribution through several iterations until convergence is reached. Density fluctuates due to temperature differences between adjacent zones, which leads to buoyancy driven flow. This phenomenon causes light hot air to rise and flow out while cooler air flows in. The system is solved by using Bernoulli's principle; taking the reference pressure on the lower boundary of the cell P_0 and according to the hydrostatic gradient, the pressure due to stack effect P_i only at height z is:

$$P_i = P_{o,i} - \rho_i g z \qquad (eq.9)$$

$$\rho_i = \rho_0 \frac{T_0}{T_0 + T_i} \qquad (eq.10)$$

where T_0 corresponds to a reference temperature and T_i the air temperature of the cell. Boundaries between volumes are written in terms of ΔP to account for the interaction between adjacent volumes. This substitution is then input into the mass conservation equation in order to satisfy the expression in equation 7 and rewritten in terms of Bernoulli:

$$\sum_{k=1}^{j} \dot{m}_{ik} = \sum_{k=1}^{j} \rho_{ik} \left[C_d W \sqrt{\frac{2\Delta P_i}{\rho_{mean}}} \right] \qquad (eq.11)$$

where C_d is a discharge coefficient inherent to the system and W the perpendicular surface to the flow. Calculation of unknown pressures is derived by application of mass balance equations in each node. The solution of the system, as stated before, is based on a Newton-Raphson iterative method. Each cell pressure is adjusted to satisfy mass balance. The new cell pressures are computed from the previous estimated pressures and a correction vector P_{corr} as follows:

$$P_{iter+1} = P_{iter} - P_{corr} \qquad (eq.12)$$

P_{corr} is calculated using:

$$P_{corr} = J^{-1}\, x\, Mb \qquad (eq.13)$$

where Mb is a mass balance vector when considering no source terms, computed by the following expression:

$$Mb_j = \sum_{k=1}^{j} Q_{ik} \rho_{ik} \qquad (eq.14)$$

and J is the Jacobian matrix calculated by:

$$J_{ij} = \frac{\partial Mb_j}{\partial P_j} \qquad (eq.15)$$

The convergence of the aerodynamic model is given by a convergence factor, which is defined by a correction vector in order to end iterations. This correction factor was set to $\varepsilon = 0.001$.

2.4 Model coupling

The data obtained in the previous sections and equation systems share information through a Matlab Simulink interface called HYBCELL (El Mankibi *et al.*, 2006, 2015) which displays the temperature evolution, pressure distribution and air flow across the chimney.

From an initial temperature distribution, aerodynamic model computes pressures and flow distributions. These results will allow new temperature calculations by changing convective heat fluxes. The model was developed to run with meteorological data from Lyon.

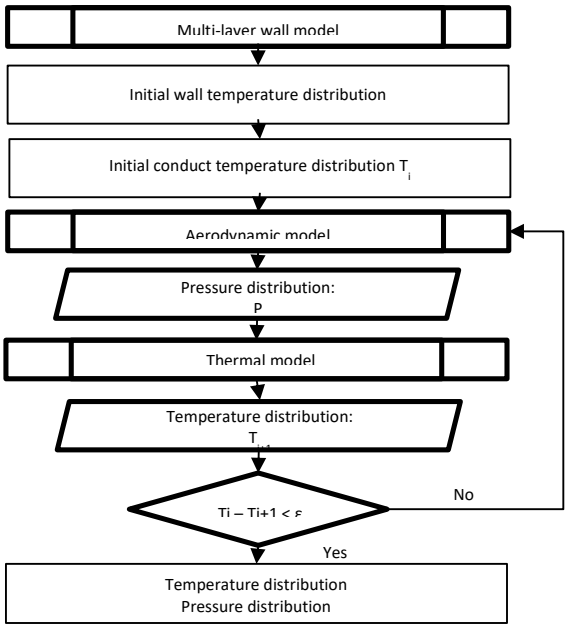

Figure 3: Flowchart of the coupled model.

3. Experimental procedure

3.1 Laboratory set-up

In order to analyze and validate the numerical models, a laboratory prototype was developed. The prototype is based on the chimney built by Acre et al. (Arce, Jiménez, *et al.*, 2009; Arce, Xaman, *et al.*, 2009) at the Almeria Solar Platform (PSA). The laboratory prototype is made from 5cm-wide polystyrene plates, supported by an aluminum beam structure (3cm cross section). The prototype is connected to one of the sections of the Guarded Hot Box (shown in Fig.3) in order to simulate the temperature in a controlled volume.

(a)

(b)

Figure 4: Laboratory prototype showing (a) the prototype and the both sides of the Hot Guarded Box and (b) ongoing experiment with PCM panels.

3.1.1 Experimental protocol

Fig. 5 below shows the protocol used for the experimentation. The experimental protocol is composed of seven consecutive phases of 6 hours each (0.25 days), completing a full cycle in roughly 1.75 days. Phases depend on the state of the opening (open/closed) for natural ventilation, and heating provided by the halogen lamps, which simulate solar radiation. The lamps are evenly distributed over the 3m glass face of the chimney and provide a net heat flux of 700 W⁄m².

Phase 1 corresponds to the initialization of the system. In this stage, the outlet is closed and there is no present heat source. Phase 2 was designed to charge the panels in order to ensure the melting process of PCMs. Phase 3 allows air circulation by opening the outlet and maintaining the heat source. Phase 4 removes the heat source while allowing air circulation. Phase 5 reinitializes the system. Phases 6 and 7 work in the same way as phases 2 and 4.

Phase 1 : Initialization

Phase 2 : Heating Only

Phase 3 : Chimney Activation

Phase 4 : Ventilation only

Phase 5 : Initialization

Phase 6 : Heating only

Phase 7 : Ventilation only

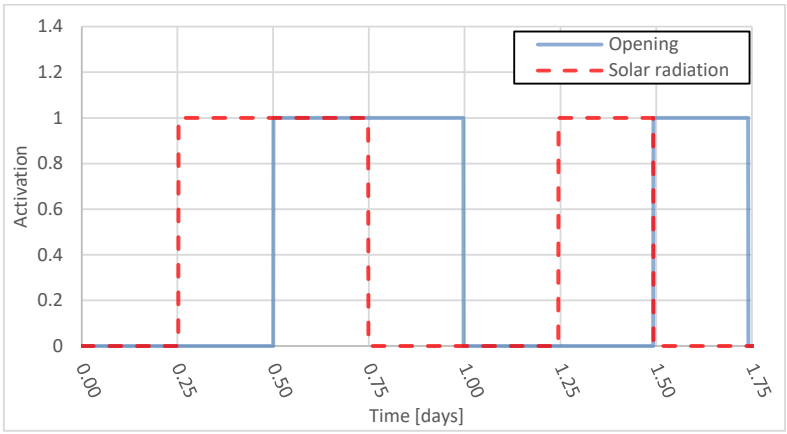

Figure 5: Experimental protocol showing the Boolean behavior between the outlet (open/closed) and the solar gain (on/off)

3.1.2 Laboratory test results

Outlet mass flow rate, air gap temperature and temperature difference between inlet and outlet, are some of the most important quantities for the design of a solar chimney. Outlet airflow for no PCM and PCM integrated solar chimney (ASC) are shown in Fig. 6-8. The results represent two continuous cycles from the experimental protocol. The results shown below were carried out under two different conditions: input temperature set by the Hot Guarded Box and no input temperature, thus following the exterior temperature.

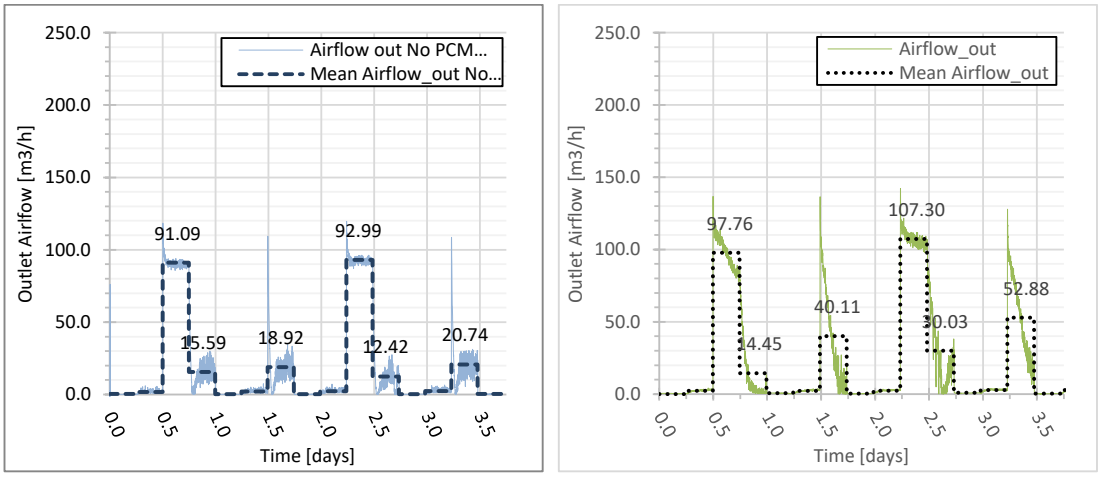

(a) **(b)**

Figure 6: Outlet airflow results for (a) 09/05/2017 No PCM Solar chimney for a set temperature of 17°C (Cycle 5 No MCP) and (b) 16/08/2017 RT44 PCM integrated Solar Chimney for a set temperature of 17°C (Cycle 4 MCP)

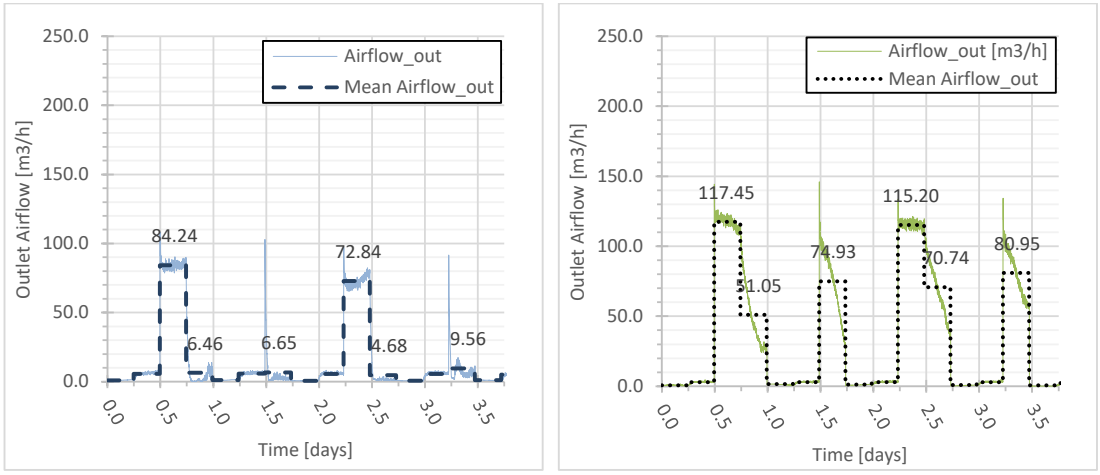

(a) **(b)**

Figure 7: Outlet airflow results for (a) 25/07/2017 No PCM Solar chimney following exterior temperature (Cycle 7 No MCP) and (b) 23/08/2017 RT44 PCM integrated Solar Chimney following exterior temperature (Cycle 5 MCP) – Max outside temperature of 42°C

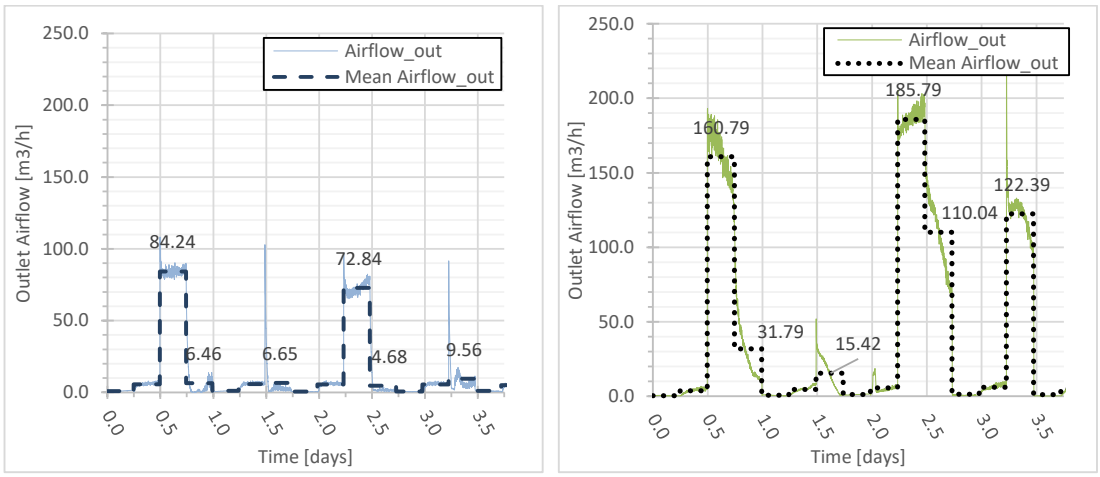

(a) **(b)**

Figure 8: Outlet airflow results for (a) 25/07/2017 No PCM Solar chimney following exterior temperature (Cycle 7 No MCP) and (b) 15/06/2017 RT44 PCM integrated Solar Chimney following exterior temperature (Cycle 3 MCP) – Max outside temperature of 45°C

The results demonstrate the influence of the different stages of the experimental protocol on the outlet mass flow rate. The impact of the PCMs is particularly noticeable during ventilation only phases (4 and 7). Solar chimney mass flow rate values drop dramatically during the aforementioned phases, as shown in Fig. 6a – 8a. The polystyrene structure provides no thermal inertia to the system, which causes a drop in outlet mass flow rate as soon as there is no longer a heat source. In turn, ASC results (as shown in Fig. 6b – 8b) display a slow decrease of mass flow rates between phases. The PCM panels work as expected, absorbing available energy during each charging phase and releasing once the source is withdrawn.

Additionally, ASC results display as well, an overall higher mean mass flow rate across all phases of the experiment. In some cases, up to a twofold increase of mass flow rate can be noted for the active solar chimney.

3.2 In-situ experimentation

The stand-alone chimney was developed in Almeria in 2009. The latest iteration of the system is 5.60 m tall, 1.20 m width and 0.52 m deep. The chimney is composed of a 0.15m thick concrete absorbing plate, thermal insulation behind the concrete plate, a 5mm thick glass cover to reduce convective and radiative losses to the environment, a wood casing, and a driving air protection; which generates a fall of pressure near the exit and,

at the same time aids the extraction of air. The prototype is shown in Fig 9. (Arce *et al.*, 2015).

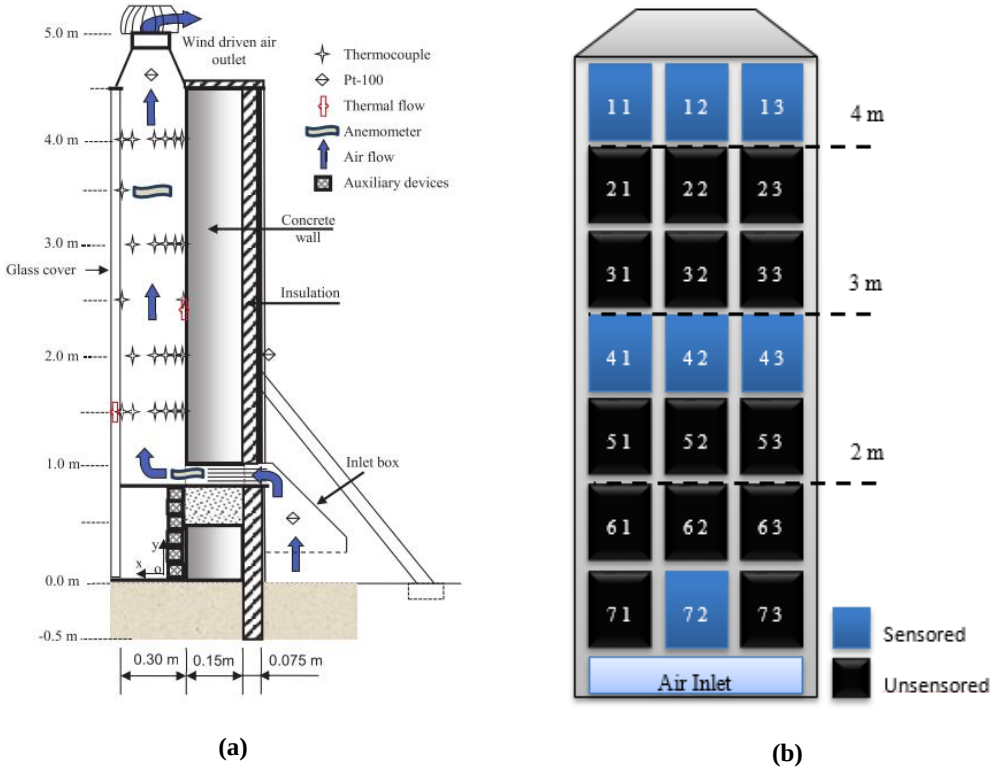

Figure 9: (a) Lateral view of the PSA solar chimney and the instrumentation set up by Arce et al. and (b) Panel distribution on the PSA solar chimney

3.2.1 PCM implementation

The dimensions of the Almeria solar chimney, as well as the cable distribution do not allow the placement of PCM panels on the perpendicular sides to the glazing. The panels are distributed over the concrete collector wall as shown in Fig. 4b in a matrix manner. The sensors are placed in the center of the panel, over and behind at three different levels: inlet panel (72) at 1,25m, center of the solar chimney (41, 42 and 43) at 2,75m and the outlet panels (11, 12 and 13) at 4,25m. The panels' southern surfaces were painted matte black in order to maximize the absorption of solar radiation and to ensure the phase change.

3.2.2 Instrumentation

The experimental instrumentation used for the different measurements of the solar chimney is detailed in the technical note published by Arce et al. (Arce, Jiménez, *et al.*, 2009). Platinum thermoresistance (PT100, 1/10 DIN) sensors are used to record surface temperature of the panels via a four-wire connection. These sensors consist of a very small sensing element embedded in a slim rubber substrate. The sensors were glued to the center of the panels as marked in Fig.9b and painted black matte to integrate them as much as possible with the corresponding surface.

A data acquisition system with the following characteristics is being used: 16-bit A/D resolution, range of measurements fitting sensor output, modules distributed to minimize wiring, based in Compact Field Point modules manufactured by NATIONAL INSTRUMENTS.

The Solar Platform of Almeria counts with its own meteorological station, which measures data ever second. Data is averaged and recorded every minute. Further details concerning the meteorological station can be found in the aforementioned article.

3.2.3 Mass flow rate

The results presented below show the exterior temperature and wind speed for the period from October 6 to

October 9 in 2016 and 2017 respectively.

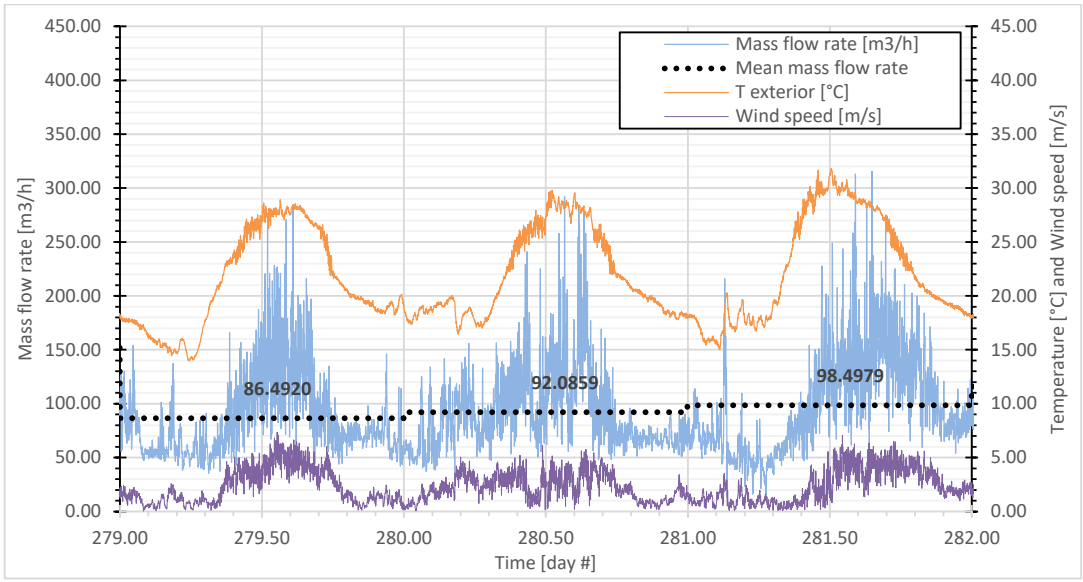

(a)

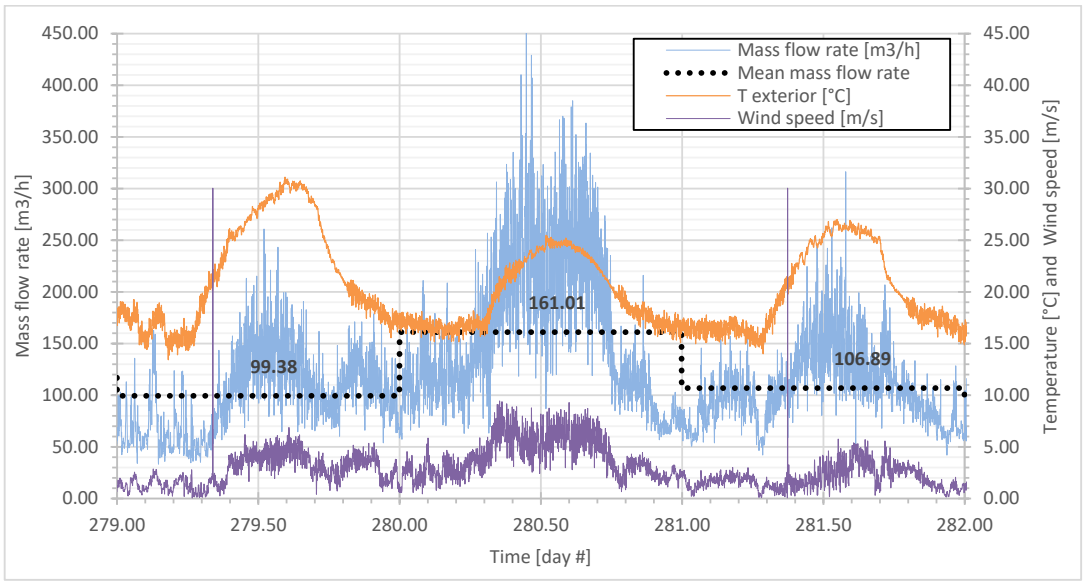

(b)

Figure 10: Influence of exterior temperature and wind speed on the mass flow rate for (a) Arce et al. solar chimney and (b) PCM integrated solar chimney

Fig. 10 (a) and (b) show an increase in mass flow rate for the PCM integrated solar chimney for the same period between both year samples. For this specific period, the overall mass flow rate is higher across the three days. The maximum and minimum differences are 62.98 m^3/h and 8.39 m^3/h respectively. The maximum temperature from the three days in 2016 is approximately 30°C, thus there is a +5°C difference in relation to the results of 2017. The highest mass flow rate values for the PCM integrated solar chimney are obtained at 25°C where wind speed has a mean wind speed of 6.5 m/s.

3.2.4 Panel surface temperature distributions

Fig. 11 (a) – (c) show the panels' surface temperature evolution for the period from October 6 to October 9 2017. In Fig. 11 (a) and (b) the phase change can be appreciated through temperature evolution of curves 12, 42 and 72 back. This phenomenon starts as soon as the temperature approaches 40°C. Once the material is fully melted temperature continues to rise until it reaches the maximum level. When solar radiation decreases

and outside temperature starts to drop, the surface temperature of the panel falls as well until it drops to 44°C. At this point, the stored energy is being released from the PCM and thus, the temperature decrease occurs at a slower rate. Moreover, Fig. 11 (c) represents the temperature evolution of the outlet level of the solar chimney. At this level, surface temperatures do not reach the phase change range. This is explained by the lack of direct sunlight due to the shadow of the top level of the solar chimney.

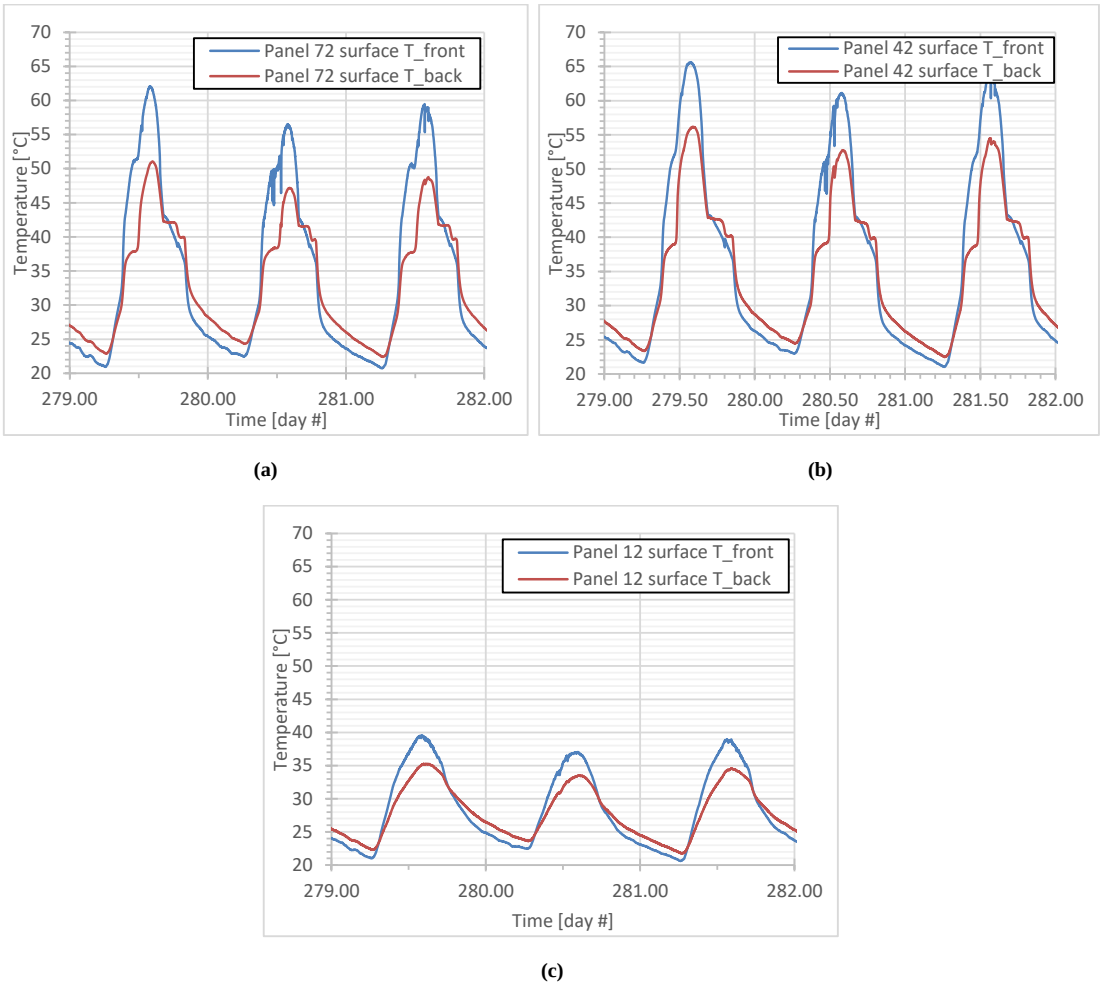

Figure 11: Frontal and back surface temperatures of the PCM panel integrated in the solar chimney at three different levels (a) inlet, (b) mid-level and (c) outlet.

4. Conclusions

An experimental study of the implementation of RT44 phase changing material panels was carried out for a solar chimney prototype under laboratory and in situ conditions. Laboratory results show a clear influence of solar radiation on the outlet mass flow rate when integrating PCMs to the solar chimney. Moreover, the interest of phase changing materials can be appreciated in these results since the mass flow rate slowly decreases once there is no longer a heat source. Outlet mass flow rate shows a steady reduction rather than the abrupt drop observed without PCM. Although the decrease is cut by the duration of each stage of the experimental protocol, its effect on mass flow rate is noteworthy. After the PCM has completed the melting process and the heat source is taken away, surface temperatures and air temperatures follow as well a slow discharge.

The increase in mass flow rate is proportional to the energy stored by the PCMs. Lower mean mass flow rates are the result of unattained melting temperatures at one or several levels of the active solar chimney. Further studies will act on the optimization of the laboratory parameters such as the heat source and the time lapses.

In situ results are yet inconclusive and require additional tests in order to validate the wind speed and melting assumptions made in order to explain the differences between the results obtained by Arce et al. and the Active

Solar Chimney. Results, even though promising, are yet to be optimized to obtain a better performance. Thus far, it can be concluded that the undercharge of the system can have an impact on the performance of the chimney. The chimney is oriented to the south; this will be particularly impactful during winter when the chimney receives an almost absolute impact of the sun. A better exposure to the sun and lower ambient temperatures will show the performance of the active solar chimneys under disadvantageous conditions.

Finally, the numerical analysis aims to describe the behavior of the phase changing materials through the combination a multi-layered wall. Further studies will emphasize in the validation of the numerical model via the experimental data obtained by both experimental procedures.

5. References

Arce, J., Xaman, J. P., *et al.* (2009) 'A parametric study of conjugate heat transfer of solar chimney', *Proceedings of the ASME 3rd International Conference on Energy Sustainability 2009, ES2009*, 1, pp. 605–612. doi: 10.1115/ES2009-90387.

Arce, J., Jiménez, M. J., *et al.* (2009) 'Experimental study for natural ventilation on a solar chimney', *Renewable Energy*, 34(12), pp. 2928–2934. doi: 10.1016/j.renene.2009.04.026.

Arce, J. *et al.* (2015) 'Thermal performance analysis of a solar chimney , based on the experimental study of the main driving variables in a physical prototype', *Paper conference*, (October), pp. 385–395.

Bansal, N. K., Mathur, R. and Bhandari, M. S. (1993) 'Solar chimney for enhanced stack ventilation', *Building and Environment*, 28(3), pp. 373–377. doi: 10.1016/0360-1323(93)90042-2.

Jianliu, X. and Weihua, L. (2013) 'Study on solar chimney used for room natural ventilation in Nanjing', *Energy and Buildings*. Elsevier B.V., 66, pp. 467–469. doi: 10.1016/j.enbuild.2013.07.036.

Kheradmand, M. *et al.* (2016) 'Experimental and numerical studies of hybrid PCM embedded in plastering mortar for enhanced thermal behaviour of buildings', *Energy*, 94, pp. 250–261. doi: 10.1016/j.energy.2015.10.131.

Li, Y. and Liu, S. (2014) 'Numerical study on thermal behaviors of a solar chimney incorporated with PCM', *Energy and Buildings*. Elsevier B.V., 80, pp. 406–414. doi: 10.1016/j.enbuild.2014.05.043.

El Mankibi, M. *et al.* (2006) 'Prediction of hybrid ventilation performance using two simulation tools', *Solar Energy*, 80(8), pp. 908–926. doi: 10.1016/j.solener.2005.08.003.

El Mankibi, M. *et al.* (2015) 'Numerical modeling of thermal behaviors of active multi-layer living wall', *Energy and Buildings*. Elsevier B.V., 106, pp. 96–110. doi: 10.1016/j.enbuild.2015.06.084.

Mathur, J. *et al.* (2006) 'Experimental investigations on solar chimney for room ventilation', *Solar Energy*, 80(8), pp. 927–935. doi: 10.1016/j.solener.2005.08.008.

Mirzaei, P. A. and Haghighat, F. (2012) 'Modeling of phase change materials for applications in whole building simulation', *Renewable and Sustainable Energy Reviews*. Elsevier, 16(7), pp. 5355–5362. doi: 10.1016/j.rser.2012.04.053.

Naraghi, M. H. and Blanchard, S. (2015) 'Twenty-four hour simulation of solar chimneys', *Energy and Buildings*. Elsevier B.V., 94, pp. 219–226. doi: 10.1016/j.enbuild.2015.03.001.

Shahreza, A. R. and Imani, H. (2015) 'Experimental and numerical investigation on an innovative solar chimney', *Energy Conversion and Management*. Elsevier Ltd, 95, pp. 446–452. doi: 10.1016/j.enconman.2014.10.051.

Zhou, D., Zhao, C. Y. and Tian, Y. (2012) 'Review on thermal energy storage with phase change materials (PCMs) in building applications', *Applied Energy*. Elsevier Ltd, 92, pp. 593–605. doi: 10.1016/j.apenergy.2011.08.025.